








RESEARCH ARTICLE | APRIL 03 2024

## Grasping the behavior of magnetorheological fluids in gradient pinch mode via microscopic imaging <sup>EP</sup>

Michal Kubík ; Jiří Žáček ; Janusz Goldasz ; David Nečas ; Michal Sedlačík ; Jiří Blahuta ; Wojciech Bańkosz ; Bogdan Sapiński 



*Physics of Fluids* 36, 042004 (2024)

<https://doi.org/10.1063/5.0203804>



View  
Online



Export  
Citation



Physics of Fluids

Special Topic:

Kitchen Flows 2024

Guest Editors: Gerald G. Fuller, Maciej Lisicki, Arnold J.T.M. Mathijssen, Endre Joachim Mossige, Rossana Pesquino, Vivek Nagendra Prakash, Laurence Ramos

[Submit Today!](#)

# Grasping the behavior of magnetorheological fluids in gradient pinch mode via microscopic imaging

Cite as: Phys. Fluids **36**, 042004 (2024); doi: 10.1063/5.0203804

Submitted: 16 February 2024 · Accepted: 16 March 2024 ·

Published Online: 3 April 2024



View Online



Export Citation



CrossMark

Michal Kubík,<sup>1,a)</sup>  Jiří Žáček,<sup>1</sup>  Janusz Gołdasz,<sup>2</sup>  David Nečas,<sup>1</sup>  Michal Sedlačík,<sup>3,4</sup>  Jiří Blahuta,<sup>1</sup>   
Wojciech Bańkosz,<sup>2</sup>  and Bogdan Sapiński<sup>5</sup> 

## AFFILIATIONS

<sup>1</sup>Faculty of Mechanical Engineering, Brno University of Technology, 616 69 Brno, Czech Republic

<sup>2</sup>Faculty of Electrical and Computer Engineering, Krakow University of Technology, 31-155 Kraków, Poland

<sup>3</sup>Centre of Polymer Systems, Tomas Bata University in Zlín, 760 01 Zlín, Czech Republic

<sup>4</sup>Department of Production Engineering, Faculty of Technology, Tomas Bata University in Zlín, 760 01 Zlín, Czech Republic

<sup>5</sup>Department of Process Control, AGH University of Krakow, 30-059 Kraków, Poland

<sup>a)</sup> Author to whom correspondence should be addressed: [michal.kubik@vutbr.cz](mailto:michal.kubik@vutbr.cz)

## ABSTRACT

Magnetorheological (MR) fluids are suspensions of micrometer-sized ferromagnetic particles in a carrier fluid, which react to magnetic fields. The fluids can be operated in several fundamental modes. Contrary to the other modes, the rheology and microstructure formation of the MR fluid in the gradient pinch mode have been studied to a far lesser extent. The magnetic field distribution in the flow channel is intentionally made non-uniform. It is hypothesized that the Venturi-like contraction is achieved via fluid property changes, leading to a unique behavior and the presence of a pseudo-orifice. The main goal is to investigate the presence of the Venturi-like contraction effect in the fluid by means of optical imaging and hydraulic measurements. To accomplish the goal, a unique test rig has been developed including a fluorescence microscope and MR valve prototype. The Venturi-like contraction hypothesis was confirmed. The results indicate that the effective flow channel size decreases by 92% at the maximum magnetic flux applied. This has a direct impact on the flow characteristics of the MR valve. The variation of the pressure–flow rate curve slope with magnetic field was demonstrated. The results provide valuable information for understanding the rheology and microstructure formation mechanism in MR fluids in the pinch mode.

© 2024 Author(s). All article content, except where otherwise noted, is licensed under a Creative Commons Attribution (CC BY) license (<http://creativecommons.org/licenses/by/4.0/>). <https://doi.org/10.1063/5.0203804>

## I. INTRODUCTION

Magnetorheological (MR) fluids are known representatives of smart materials.<sup>1,2</sup> The material itself is a suspension of micrometer-sized ferromagnetic particles in a non-conductive carrier oil. While in the presence of magnetic field, it undergoes a fast and reversible transition from a liquid to a pseudo-solid. The magnetized particles form chain structures (cluster) orientated in the direction of magnetic flux. On a macro-scale, the formation of the chain structures in the material translates into yield stress increase.<sup>3</sup> The result is a resistance-to-flow change. The controllable property attracted interest from several industries, and effectively, the technology has been used in automotive vehicle semi-active suspension MR dampers,<sup>4</sup> powertrain mounts,<sup>5</sup> or high-quality optical finishing systems.<sup>6</sup>

The MR fluid can be operated in one of the fundamental modes:<sup>7</sup> valve, shear, squeeze, and gradient pinch mode. In the *valve mode*

(flow mode), the surfaces constituting the flow channel are stationary, and the magnetic flux is applied in the direction perpendicular to the fluid flow—see Fig. 1(a). The flow through the valve is initiated once the yield stress (or breakaway pressure) is overcome. The configuration is typical for long-stroke vehicle suspension dampers<sup>8</sup> or powertrain mounts.<sup>5</sup> For comparison, the shear mode features a flow channel with surfaces moving relative to each other. Exemplary *shear mode* hardware includes MR brakes<sup>9</sup> or clutches.<sup>10</sup> Again, the induced magnetic flux is arranged perpendicularly to the motion direction. Next, *squeeze-mode* devices are capable of developing high pressure gradients upon a relatively small input displacement span; the height of the flow channel in such valves varies according to the prescribed displacement or force. As in the previously considered modes, the magnetic flux is orientated in the perpendicular direction to the fluid flow (or in parallel with the prescribed input motion direction).

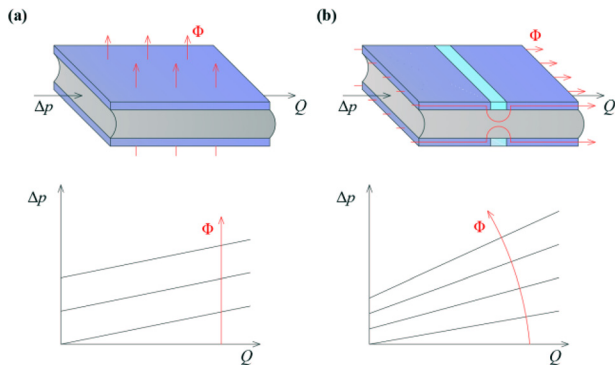


**FIG. 1.** MR fluid fundamental modes: (a) flow and (b) gradient pinch;  $Q$ —flow rate,  $\Delta p$ —pressure drop, and  $\Phi$ —magnetic flux. Gray areas denote MR fluid, blue regions refer to magnetic materials, and cyan zones are non-magnetic.

It is best suited for small displacement uni-directional vibration mounts.<sup>11</sup> The *gradient pinch mode* stands out from the crowd in the operating mode context, as shown in Fig. 1(b). First, the magnetic flux distribution in the flow channel is intentionally *non-uniform*. Second, the magnetic flux that is induced in the structure flows through the gap in the direction parallel to the fluid flow direction and in between the neighboring magnetic pole pieces. The effect is that the largest magnetic flux concentration is located in the regions adjacent to the flow channel walls and low (ideally zero) in the center of the gap. The effect is a Venturi-like contraction to be achieved via material property changes. Finally, only a small volume of the fluid is energized, whereas the MR fluid operation in the other modes involves activating the entire volume of the material in the flow channel.

Contrary to the other operating modes, the rheology of the MR fluid in the pinch mode has been studied to a far lesser extent. Few notable examples can be related to, e.g., Goncalves and Carlson,<sup>12,13</sup> who were the first to describe the pinch mode fundamentals; however, only a few details were provided. They also made a basic attempt to relay the resulting pressure drop  $\Delta p$  to the input flow rate through the pinch valve  $Q$ .<sup>12</sup> That was accomplished on the basis of the simple Wuest equation to relate the pressure drop and the flow rate as  $\Delta p = kQ$ , where for a rectangular slit of the depth  $h$  and the height  $D$  (see Fig. 2)<sup>14</sup> the coefficient  $k \sim 32\mu/\pi D^2 h$ ,  $\mu$ —viscosity and  $k$ —proportionality constant. This equation is valid for laminar flow and  $h \gg D$ . As demonstrated by the researchers, the coefficient  $k$  increased with magnetic flux due to the degradation of the effective flow area. Next, Góldasz and Sapiński<sup>15</sup> carried out a basic magnetostatic analysis of several pinch mode valve configurations with thru-hole type flow channels. In the CFD (computational fluid dynamics) study, Góldasz

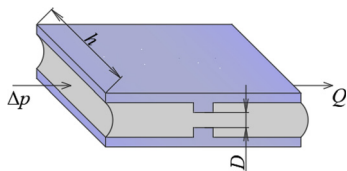


**FIG. 2.** Rectangular slit-type orifice;  $h$ —channel depth and  $D$ —channel size.

*et al.*<sup>16</sup> analyzed several pinch mode scenarios. The theoretical analysis involved several valve configurations and magnetic flux (or yield stress) arrangements. Moreover, the authors commented on the possible existence of the pinch mode flow’s upper limit. Moreover, Kubik *et al.*<sup>17</sup> executed an extensive experimental study with several MR fluid formulations and a single-stage MR pinch valve. Briefly, the authors obtained optimum results with the lowest Fe vol. concentration fluid. Lee *et al.*<sup>18</sup> developed a basic MR pinch valve with an annular channel and derived a mathematical model of the fluid’s behavior subjected to non-uniform magnetic field inputs. This loading mode has also been used in rotary<sup>19</sup> and linear seals.<sup>20</sup> Finally, Kuzhir *et al.*<sup>21</sup> examined the flow of a suspension of micrometer-sized non-magnetic particles in a ferrofluid through a capillary channel under the influence of magnetic field generated by permanent magnets. The authors examined various arrangements of the field with the respect to the fluid flow and showed that the effect of longitudinal field results in a significant increase in the slope of the pressure–flow rate curves.

Based on the outcome of the prior research, several key conclusions can be drawn. First, utilizing the pinch mode in valves results in an unusual behavior (compared to the other modes) manifested by variations of the pressure–flow rate curve with magnetic field (or current); see Fig. 3. Effectively, the dynamic range (defined in absolute terms as the difference between the off-state pressure drop at a given flow rate and the corresponding pressure drop in the activated state) increases with flow rate. The effect is likely due to the particle micro-structure formation in the flow channel (semi-solid regions formed by agglomerated particles in the control volume adjacent to the magnetic pole surfaces). The presence of the contraction in the flow channel is due to the balance between the hydrodynamic forces and the magnetic forces. Now, the magnetic flux depends on position in the activated region, so a force which draws the ferromagnetic particles into areas where the magnitude of the field reaches maximum. Next, no real-world prototypes have been developed so far.

The operation of existing prototypes of MR pinch valves is limited to small-scale laboratory tests, and few were characterized sufficiently enough to draw sound conclusions. At present, the magnitude of output of the pinch mode prototypes is rather moderate.<sup>12,17,18</sup> Also, arranging the active sections of the valve in series amplifies the output of the valve, however, at a cost of increased energy consumption. Briefly, search for optimum MR pinch mode valve configurations continues. To the best knowledge of the authors, no major progress in the

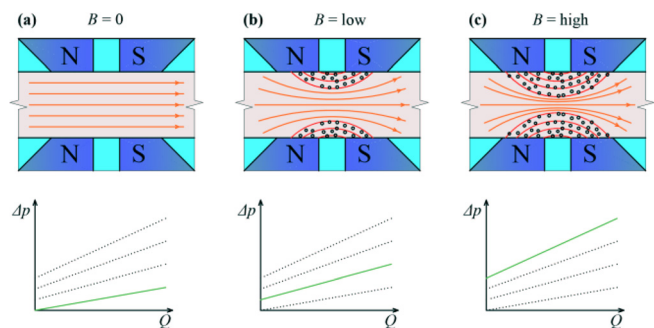


**FIG. 3.** Anticipated mechanisms of MR fluid operating in the pinch mode; (a) no magnetic flux, (b) low magnetic flux, and (c) high magnetic flux; orange—fluid streamlines, red—magnetic flux lines, and gray—MR fluid.

field is possible unless *key mechanisms governing the microstructure formation in the activated zones are examined and fully understood*. That can be exploited either via modeling studies on a micro-scale or experimental studies. Meso-scale modeling of the interactions between the particles and the fluid in the presence of non-uniform magnetic fields is, however, complicated by the fact that the magnitude of the magnetic gradient forces depends on position. As the particles are drawn to the areas with the highest magnetic field, their local concentration in the fluid's control volume varies with the position, too. Consequently, the meso-scale methods, which are based on the assumption of continuous media, are likely to fail in providing reliable estimates of the MR pinch effect. For instance, Goldasz *et al.*<sup>22</sup> studied the flow of an MR fluid through a planar channel in the pinch mode using a one-way weakly coupled CFD-FE (computational fluid dynamics, finite element) code and by means of the apparent viscosity approach. The research has succeeded in part, i.e., the study underestimated the magnitude of the pinch effect but the observations of the velocity profiles in the active region led to a conclusion that it was likely due to underestimated shear stresses in the near-wall sections of the channel. Therefore, it seems that one optimal approach to proceed is to acquire the knowledge from micro-level (modeling or laboratory) studies from which the information can be acquired, synthesized, and extrapolated.

In this study, the authors employ fluorescence microscope to visualize the behavior of the MR fluid exposed to non-uniform magnetic field distributions in an effort to gain knowledge through visual observations of the fluid's behavior. Experimental microscopic studies are relatively rare contrary to numerous particle-level 2D/3D simulations of the MR fluid microstructures, to name only.<sup>23,24</sup> For instance, Wang *et al.*<sup>25</sup> studied the microscopic characteristics of an MR fluid in low magnetic fields (up to 12 mT) by means of the industrial computed tomography (CT). The study was based on a 30% Fe vol. MR fluid. Next, Shen *et al.*<sup>26</sup> used confocal laser scanning microscope to visualize the MR fluid's microstructure and comprehend its rheological behavior. The study was executed using an MR fluid with the Fe vol. of 0.2% (maximum stated concentration). The magnetic field was generated by means of a permanent magnet. Dongshen *et al.*<sup>27</sup> used a metallographic microscope to study the MR fluid's microstructure of 30% Fe vol. Finally, Ocalan and McKinley<sup>28</sup> used an inverted microscope with a monochromatic CCD camera. They studied the aggregation dynamics of MR fluid particles and the evolution of the microstructure under the influence of pressure-driven flow. They stated that the Mason number significantly affects the average cluster size. The experiments were performed using an MR fluid with an average volume particle concentration of 0.01%. The authors dealt with uniform distributions of magnetic field and their influence on the rheology of the suspension. There is a need then to gain a detailed insight into the ferromagnetic particle microstructure in the presence of non-uniform magnetic field distributions using optical or computed tomography (CT) methods.<sup>26,28,29</sup> Here, the authors carry out the research by employing fluorescence microscopy to accomplish the research goals. Confocal microscopy, fluorescence microscopy, and scanning laser confocal microscopy are imaging techniques widely used in biological science. The fluorescence method is noninvasive, thus permitting observations of various samples, even the living ones. Owing to observations of the experimental data, the *authors hypothesis* is that a *pseudo-orifice is formed due to MR fluid exposed to non-uniform*

(longitudinal) *magnetic field* by attracting the particles to the channel walls where the largest magnetic flux density can be achieved and the smallest (ideally zero) in the center of the flow channel. Moreover, the presence of the agglomerates can be directly linked to the pressure-flow rate curve slope change manifested experimentally.

## II. MATERIALS AND METHODS

### A. Test rig

The test rig illustrated in Fig. 4 incorporates a stepper motor driven syringe pump, an MR pinch valve prototype, and a fluorescence microscope. The simple pump involves a pair of the plastic syringes (1), both, respectively, connected to the inlet and the outlet of the MR pinch valve by means of the plastic hoses (3). The motion of the syringes was imposed by a stepper-motor controlled by the driver (2). The valve was composed of the two solenoids (4). Each solenoid incorporated the coil assembly (5), the core (6), the planar flow channel (air gap) (8) for the MR fluid (7) to pass through. The glass cover (air gap) (8) for the MR fluid (7) to pass through. The glass cover was sealed by a 0.3 mm thick NBR rubber element. The purpose of the glass cover (placed directly above the active zone) was to allow for capturing the motion of the fluid in the active zone by means of a fluorescence microscope. The active zone was  $w = 3$  mm wide and  $h = 1.5$  mm deep. The distance between the neighboring magnetic poles is  $s = 1$  mm. The magnetic circuit's specific dimensions were determined using FE (finite element) magnetic calculations and with regard to the already developed geometry of the MR rheometer revealed in Refs. 17 and 30. Figure 4 shows the details of the active zone including the magnetic field lines in the flow channel (9) and the particle clusters (10) drawn for the purpose of illustration only. A fluorescence microscope was used to visualize the formation of the particle clusters in the active zone in the flow channel. The microscope's system incorporates the following elements: UV light source, camera,

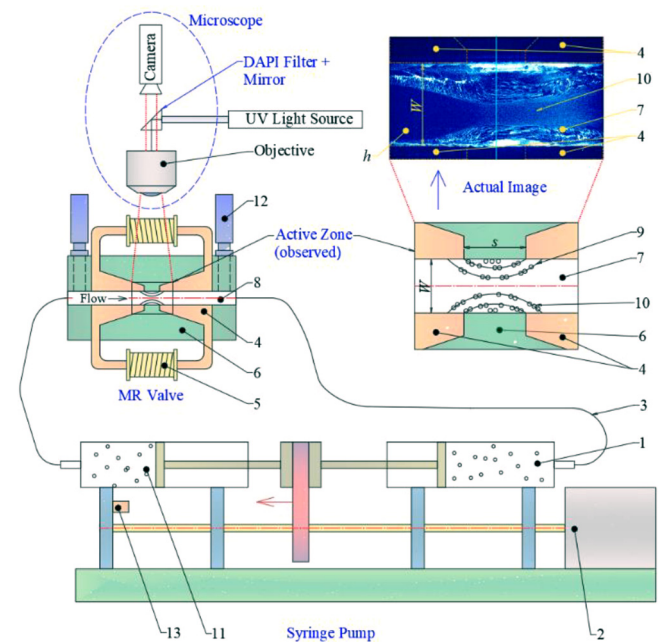


FIG. 4. Layout of the test rig.



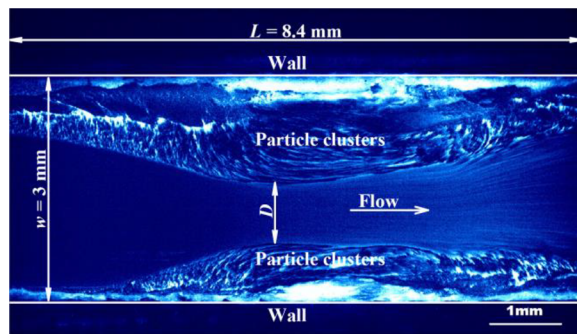


FIG. 5. Illustration of the active zone—scanned image;  $D$ —pseudo-orifice size,  $w$ —channel wide, and  $L$ —scanned length.

DAPI filter (excitation filter, dichroic mirror, and emission filter), glass plate, and an objective. Moreover, as seen in Fig. 4(a), representative example of the scanned area of the active zone can be observed.

It must be noted that this is an image of the surface of the scanned area as revealed in Fig. 5. However, based on the information obtained during a series of preliminary tests, the authors concluded the collected data were representative and can be used for further analyses. The flow conditions in the channel were those of a typical planar flow, and it can be assumed that the observed formation in the top view was further reproduced deep into the channel. The test rig was adapted to fit the two pressure sensors (12) for online measurements of the pressure drop across the valve. The position and the velocity of the syringe pistons were also monitored (13).

## B. Magnetorheological fluid composition and properties

To carry out the microscopic observations, an in-house MR fluid was prepared by the authors. Unfortunately, commercially available MR fluids could not be used due to the inconformity of the carrier fluid. As a result, the fluorescent images could not be obtained if the commercial MR suspensions have a different carrier fluid than mineral oil. The composition of the in-house prepared MR fluid was as follows: (i) OL-J3 carrier mineral oil supplied by Paramo, (ii) BASF CIP HQ (mean particle size distribution: 2–5  $\mu\text{m}$ ) iron particles—22 Fe vol%, (iii) CLAYTONE 40 anti-sedimentation additive—1.9 vol. %, and (iv) propylene carbonate activator for the additive—0.8 vol. %. Both additives (CLAYTONE 40 and propylene carbonate) were added to ensure the sedimentation stability of the suspension to maintain the concentration of the particles to be uniform throughout the fluid's volume. The apparent viscosity of the carrier fluid (OL-J3) was measured to be 0.0051 Pa s at  $T = 40^\circ\text{C}$ .

To characterize the in-house MR fluid, its fundamental characteristics were measured using the Anton Paar MCR 301 magnetocell. The results are illustrated in Fig. 6. During the tests, the shear rate was varied from 0.01 to 1000 1/s and the magnetic flux density from 0 to 800 mT. In off-state (no magnetic field), this MR fluid sample exhibited dynamic yield stress of 13 Pa and a Bingham viscosity of 0.056 Pa·s at  $22^\circ\text{C}$ .

## C. Experiment setting and test plan

A fluorescence microscope was used to conduct these measurements and to observe the microstructure formation inside the active zone.

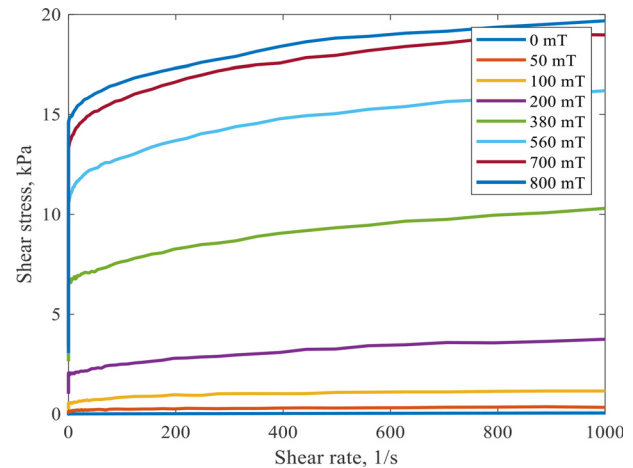


FIG. 6. In-house MR fluid measurements: shear stress vs shear rate.

The widefield epi fluorescence microscope with a monochromatic camera (model: Andor DC-152Q-COO-FI by Oxford Instruments) for recording pictures and videos throughout the experiment, was employed. The scanning frequency was 50 Hz. The illumination was provided by a UV lamp ThorLabs Solis-365C with the wavelength of 365 nm. This device was used with a  $2\times$  scope objective (Nikon Plan  $2\times/0.06$  WD 7.5) for scanning the entire width of the active zone (scanning area dimensions:  $8.4 \times 4.7 \text{ mm}^2$ ). The resolution of the obtained pictures was  $2560 \times 1460$  pixels. Given the observed area dimensions, single pixel dimensions are  $3.25 \times 3.25 \mu\text{m}^2$ . To measure the pressure drop, two pressure sensors B&K HBM P8AP with pressure range up to 10 bars, were used. The sensors were located near the entrance and the exit of the active zone of the pinch MR valve. The position sensor Micro Epson wps-150-mk30-p25 was used for acquiring the displacement of the syringe's piston. The flow rate was determined based on the syringe's piston cross section area and the position (velocity) data. All measured signals were recorded using the Dewesoft DAQ system DEWE 50.

The series of the measurements was performed at five fixed coil total current levels,  $I = \{0, 1, 2, 4, 6\}$  A, and four maximum flow rates,  $Q = \{0.16, 0.75, 1.30, 1.95\}$  ml/s, by energizing the parallelly connected electromagnetic coils and applying the prescribed displacement input to the syringes. It should be noted that the flow rates could vary slightly from one measurement to another. In order to ensure the repeatability of the experiments, the measurements were repeated three times and then averaged. All pictures and videos were recorded during the experiments simultaneously with the pressure and flow rate measurements. Thus, the micro-level observations can be linked directly to the characteristics and the behavior of the fluid in flow through the pinch valve.

## D. Data post processing

The width  $w$  of the flow channel and the pseudo-orifice width  $D$  were measured based on non-compressed versions of the acquired images. The formula for calculating the width is straightforward. The resolution of the camera is  $6.5 \mu\text{m}$ , given that fact, the optics with  $2\times$  magnification factor was used (lower magnification was needed to

observe the full width of the slit), and the formula for calculating the width  $w$  is then as follows:

$$w = (\text{No. of pixels} * 0.0065) / \text{magnification}. \quad (1)$$

With the current setup of the fluorescence microscope, it is not possible to observe individual particles but clusters. However, it is sufficient as the underlying goal was to observe the formation of the particle clusters along the entire length of the active zone. Figure 5 highlights the key dimensions. The size of the pseudo-orifice width  $D$  in the active zone was then determined based on the information extracted from the images. Determining the dimension was straightforward as the interface between the stationary agglomerates and the flowing MR fluid is sharp. Next, as already mentioned, the pressure drop across the channel was calculated given the pressure measurements at the entrance and the exit of the channel, respectively. The entire measurement took 6 s. The presented data were obtained by averaging the pressures across the last  $\Delta t = 3$  s timespan due to fluid flow stabilization. To determine the relationship between the input flow rate  $Q$  through the valve and the resulting pressure drop, the linear regression model was applied to the acquired results as follows:

$$\Delta p(\phi, Q) = k(\phi)Q + \Delta p_\tau(Q), \quad (2)$$

where  $\Delta p(\phi, Q)$  refers to the resulting pressure drop,  $k(\phi)$  denotes the pressure–flow rate curve slope at a given magnetic flux level  $\phi$  (or the coil current  $I$ ), and  $\Delta p_\tau$  is the pressure offset. To normalize the slope factor  $k$  change with magnetic flux, the dimensionless slope factor  $K$  was introduced in the following form:

$$K(\phi) = k(\phi)/k(0). \quad (3)$$

The linear regression model was selected to allow for a simple comparison of the measured data with the results published in Ref. 17.

### III. RESULTS AND DISCUSSION

#### A. Flow visualization

Figure 7 (Multimedia view) reveals the image of the flow channel at off-state conditions ( $I = 0$  A). Next, Fig. 8 (Multimedia view) highlights flow conditions at the maximum magnetic field ( $I = 6$  A). As observed, at the off-state condition the channel still contains tiny clusters of particles. It is likely due to the residual magnetic flux. Unfortunately, efforts to completely demagnetize the magnetic circuit

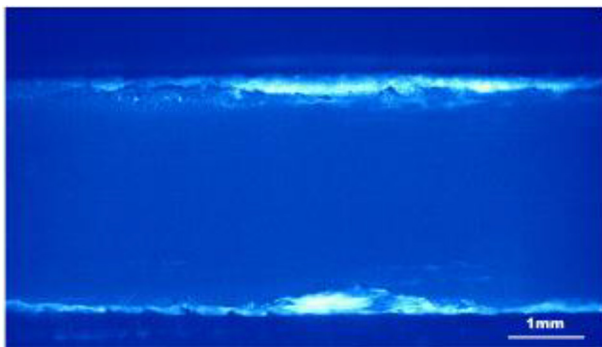


FIG. 7. Flow channel: off-state, no magnetic flux ( $I = 0$  A,  $\Phi = 0$  mWb,  $Q = 0.16$  ml/s). Multimedia available online.

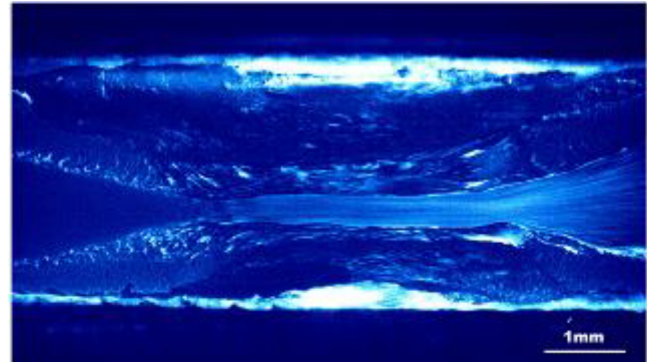


FIG. 8. Flow channel: maximum magnetic field ( $I = 6$  A,  $\Phi = 3.54$  mWb,  $Q = 0.16$  ml/s). Multimedia available online.

did not succeed in full. Figure 8 (Multimedia view) also shows the pseudo-orifice  $D$  developed by the particle clusters at the highest magnetic flux  $\Phi$  (corresponding to the maximum total current  $I = 6$  A). To supplement the material, the results of the magnetostatic modeling of the pinch valve can be found in the Appendix.

The stationary clusters and the moving fluid can be clearly observed in the image. It appears that the minimum pseudo-orifice occurs not in the middle of the channel but near the entrance. This corresponds to the magnetic flux distribution shown in the Appendix and with the well-known phenomenon of *vena contracta*, observed in Newtonian fluids. Ocalan and McKinley<sup>28</sup> dealt with the problem of MR fluid flow contraction and expansion in the valve mode. In the referenced study, non-uniform magnetic field occurred at the entrance to the gap, and their results cannot be directly compared with those obtained by the authors. Next, Kuzhir *et al.*<sup>31</sup> studied the behavior of MR fluid in flow through a channel in series with a circular orifice and in the presence of magnetic field. The researchers drew several hypotheses on the presence of non-uniform magnetic fields at the entrance to the orifice. Again, the results cannot be directly compared with the present data.

The videos are the primary output of the visual experiments. The videos illustrate that the whole process and the pseudo-orifice shape and size are relatively stable under the testing conditions. However, a significant layer of moving clusters can be seen at the entrance and exit to the pseudo-orifice. Moreover, the pseudo-orifice is asymmetric, i.e., the upper cluster is slightly thicker than the lower one. The asymmetry is minor and is likely to be due to slightly different magnetization characteristics of the two solenoids.

#### B. Magnetic field effect

Figure 10 contains a series of images collected during the experiments. The columns in Fig. 10 contain the recorded images of the fluid flow at different levels of magnetic flux (or coil current) and equal flow rates. The images were basis for the measurements of the width of the pseudo-orifice  $D$ . It is evident that as the magnetic flux increases, the size of the pseudo-orifice  $D$  decreases (at a given flow rate  $Q$ ). The relationship is non-linear. The pseudo-orifice width  $D$  is relatively stable as seen in the error bars in Fig. 9. No trends associated with the pseudo-orifice size variance were observed during the experiments. Based on the data in Fig. 10, it can be concluded that the magnetic field



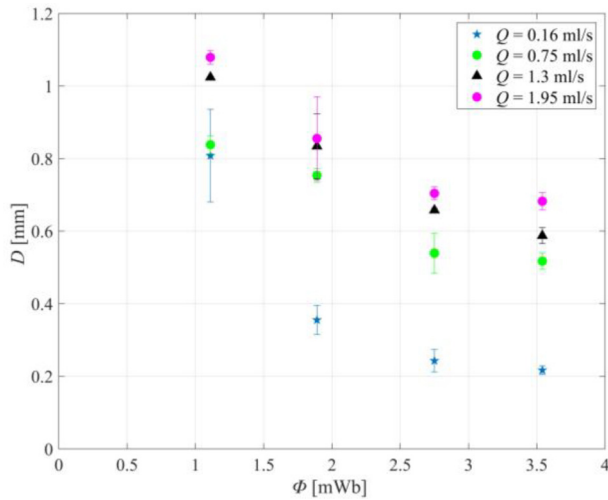


FIG. 9. Flow channel: maximum magnetic flux ( $I=6$  A,  $\Phi=3.54$  mWb,  $Q=0.16$  ml/s).

significantly affects the width of the pseudo-orifice  $D$ . The higher the magnetic field is developed in the solenoid, the smaller the size of the pseudo-orifice  $D$  is.

It can be stated that an external non-uniform magnetic field affects the size of the pseudo-orifice  $D$  at a constant flow rate  $Q$ . In the examined case, the pseudo-orifice size decreased from 3 mm ( $\Phi=0$  mWb) down to 0.22 mm ( $\Phi=3.54$  mWb) at the flow rate  $Q=0.160$  ml/s.

This confirms the pinch mode hypothesis expressed by Goncalves and Carlson,<sup>12</sup> Lee *et al.*,<sup>18</sup> or Kubík *et al.*<sup>17</sup> at least within the tested flow rate range (0–1.95 ml/s) and the magnetic flux range (0–3.54 mWb). Moreover, the relationship between the size of the pseudo-orifice and the pressure–flow rate curve slope change can be easily deduced from the experimental data.

### C. Flow rate effect

The rows in Fig. 10 are images of the fluid at the various flow rates  $Q$  and equal magnetic flux levels. Based on the observations of the images, it can be concluded that as the flow rate  $Q$  increases, the width of pseudo-orifice  $D$  increases. Again, this relationship is non-

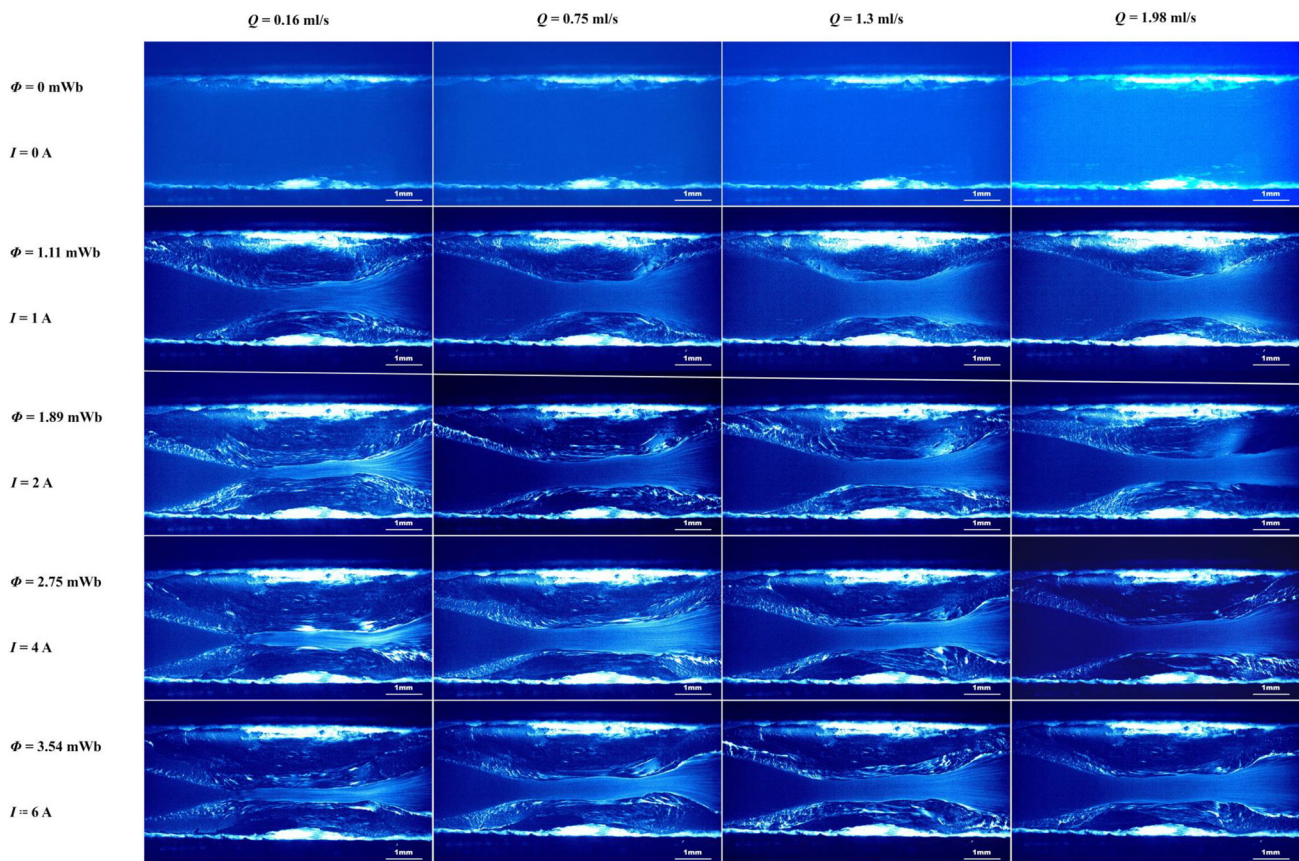


FIG. 10. Effect of magnetic flux  $\Phi$  and flow rate  $Q$  on the pseudo-orifice size  $D$ .

linear. It is expected that the pseudo-orifice size  $D$  is due to the balance between drag (viscous) forces and magnetic forces. This statement is supported by the authors' previous measurements with various MR fluids with significantly higher carrier fluid viscosities when no change in the pressure–flow rate curve slope was observed. The authors calculated the highest average flow velocity in the pseudo-orifice to be 1.5 m/s ( $\Phi = 3.54$  mWb and  $Q = 1.95$  ml/s).

**D. Flow characteristics**

Figure 11 shows the plots of pressure drop vs flow rate  $\Delta p$ – $Q$  at different levels of magnetic flux. It is evident that the change in the pseudo-orifice size  $D$  leads to a change in the slope of the  $\Delta p$ – $Q$  curve of the valve, as shown in the graph. It can be observed in Fig. 11 that the off-state pressure drop at zero flow rate showed an offset of 0.033 bar. It is likely due to the residual magnetic flux in the magnetic circuit or anti-sediment CLAYTONE 40 additive in the in-house MR fluid that increases the fluid's yield stress in the non-activated state. As the magnetic flux increases, the slope follows the trend, too. The data have been fitted with a simple linear regression model that is described in Sec. II D. The dimensionless slope factor  $K$  was then determined based on the datasets. In the examined case, the slope factor was found to be  $K = 1.78$ . This is significantly lower than in the case of prior works: Goncalves and Carlson<sup>12</sup>— $K = 6$  (est.), Lee *et al.*<sup>18</sup>— $K = 17$  (est.), Kubik *et al.*<sup>17</sup>— $K = 6.6$ , or Žáčec *et al.*<sup>32</sup>— $K = 9$ . It is likely that the main cause of the relatively low slope factor is the different geometry of the flow channel (planar slit vs circular thru-hole in Ref. 17). Thus, the contribution of the magnetic forces to the pseudo-orifice comes from the top and bottom surfaces of the flow channel. It should be also noted that the measured data were fitted with the simplest linear model. This is to allow for a straightforward comparison with the prior data.<sup>17,18,32</sup> However, in the examined case, each series of data collected at a given magnetic flux includes only four data points. It is problematic then to draw firm conclusions from the acquired populations as to the definite trend. The authors conclude that the whole process is relatively stable and well-repeatable, although the findings slightly deviate from the results obtained in<sup>17</sup> based on laboratory

experiments with a pinch MR valve on a hydraulic pulsator. In that study, the authors tested the valve under significantly higher magnetic flux levels and significantly higher flow rates (up to 166 ml/s) using commercially available MR fluids with a number of additives, which may significantly influence the rheology of the material. In the present case, a commercially available MR fluid could not be used in the experiments due to its incompatibility with the visualization method requirements. Another difference is in the method of excitation (constant acceleration input). In this project, the fluid flow was forced at a constant flow rate (constant velocity of the syringe). It can be expected that as the flow rate increases, the pseudo-orifice size will degrade, leading to unstable behaviors. That is one definite subject of further research.

The exploited method yields valuable results. However, its main limitation is the ability to observe only the surface of the active zone. Direct observations of the internal microstructure are not possible with this approach. Therefore, the authors can only deduce or extrapolate the observations to the inner volume of the MR fluid. Thus, all presented results must be interpreted in this way, and this limit must be considered. One alternative to provide an insight into the internal microstructure of the MR fluid is the computed tomography method; however, it is only capable of static images.

On a different note, it is important to point to another limitation. The paper reveals the results of a finite-element magnetostatic study to examine the non-uniform magnetic field distribution in the active zone. With the model, MR fluid properties are assumed to be time-invariant and homogenous in the control volume. However, it can be expected that the magnetophoretic forces<sup>28,33</sup> will cause the migration of particles due to the magnetic flux density gradient. Therefore, the concentration of ferromagnetic particles (density) in the active zone is not constant, and the magnetic properties are volume dependent. Such insight can be provided with particle-level models. According to the best knowledge of the authors, no modeling studies dealing with the micro-level motion of the particles in the pinch mode have been published so far. Other research studies on the pinch mode omit this phenomenon as well.<sup>18</sup>

**IV. CONCLUSIONS**

The paper deals with the behavior of an MR fluid in the presence of non-uniform magnetic fields in the pinch mode. It was hypothesized that in such conditions, MR fluids develop Venturi-like contractions via material property changes (yield stress), leading to the formation of a pseudo-orifice. To understand this phenomenon, a test rig and a pinch mode MR valve were developed. A fluorescence microscope was used to conduct these measurements and to observe the microstructure formation. The key conclusions are as follows:

- The hypothesis on the pseudo-orifice formation in the MR fluid subjected to non-uniform magnetic fields was confirmed. In the examined case, the pseudo-orifice size decreased from 3 mm ( $\Phi = 0$  mWb) down to 0.22 mm ( $\Phi = 3.54$  mWb) at the flow rate of  $Q = 0.16$  ml/s.
- The pseudo-orifice size  $D$  is dependent on magnetic flux  $\Phi$  and flow rate  $Q$ . As the magnetic field increases, the size of the pseudo-orifice  $D$  decreases (at a given flow rate  $Q$ ), see Figs. 9 and 11. The relationship is non-linear. As the flow rate  $Q$  increases, the width of the pseudo-orifice  $D$  increases. Again, this relationship is non-linear.

01 August 2024 08:35:36

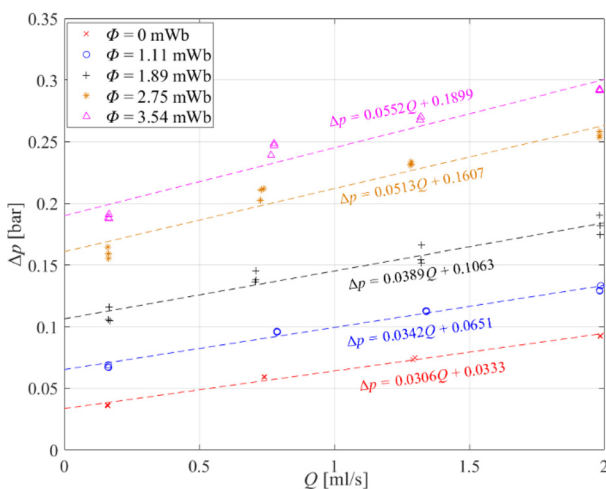


FIG. 11. Pressure drop  $\Delta p$  vs flow rate  $Q$  and magnetic flux  $\Phi$ .



- The relationship between the size of the pseudo-orifice  $D$  and the pressure–flow rate curve slope change was confirmed experimentally within the specified test range.

Finally, the study confirms the microstructure formation phenomenon (key principle of the gradient pinch mode) via experimental means. The authors believe that the findings pave way toward applications of the gradient pinch mode in microfluidics or controlled valves with the unique controlled slope characteristics. However, to gain a more detailed insight and lay grounds for the optimization of this phenomenon in MR devices, micromechanical modeling studies are needed. That step is planned in the near future.

## ACKNOWLEDGMENTS

The authors wish to acknowledge the kind support of the Czech Science Foundation (Grantová agentura České republiky—GACR) and the National Science Centre (Narodowe Centrum Nauki—NCN, Poland)—Grant Nos. GACR 21-45236L (CZ) and 2020/39/I/ST8/02916 (PL).

## AUTHOR DECLARATIONS

### Conflict of Interest

The authors have no conflicts to disclose.

### Author Contributions

**Michal Kubík:** Conceptualization (equal); Methodology (equal); Resources (equal); Supervision (equal); Writing – original draft (equal); Writing – review & editing (equal). **Jiří Žáček:** Conceptualization (equal); Data curation (equal); Investigation (equal); Methodology (lead). **Janusz Gołdasz:** Conceptualization (equal); Supervision (equal); Writing – original draft (equal); Writing – review & editing (lead). **David Nečas:** Resources (equal); Writing – review & editing (supporting). **Michal Sedlačík:** Validation (equal); Writing – review & editing (equal). **Jiří Blahuta:** Data curation (supporting); Visualization (equal). **Wojciech Bańkosz:** Investigation (equal); Software (equal). **Bogdan Sapiński:** Conceptualization (lead); Methodology (equal); Project administration (lead).

## DATA AVAILABILITY

The data that support the findings of this study are available from the corresponding author upon reasonable request.

## APPENDIX: MAGNETIC CIRCUIT CHARACTERIZATION

### 1. Magnetic circuit

The purpose of developing the magnetostatic model was (1) to size the solenoids in MR valve and (2) to gain insight on the distribution of the magnetic field in the active zone. The magnetostatic 3D analysis was performed in Ansys Electronics Desktop 2023 R1. Figure 12 reveals the simplified geometry of MR pinch valve magnetic circuit for the FE models. The following material properties were assumed for the specific components in the circuit: orange—low-carbon alloy steel 11SMn30, blue—MR fluid, green—bronze or aluminum, and gray—copper. The mesh size in the active zone (flow channel and pinch gaps) was set to be equal to 0.2 mm, and in the remaining portion of the solenoid, it was set to 0.5 mm. The magnetization curve dataset in Ref. 19 was used. The coil was wound with 200 turns of copper wire.

### 2. Search coil measurements

Magnetic flux measurements were carried out using the search coil approach. In addition to the primary coil of 200 wire turns, each assembly featured a search coil (150 turns of 0.3 mm wire) wound below the primary coil. The search coil senses the average flux passing through the core. As such, it is known to obtain the flux linkage data by integrating the voltage induced in the search coil.<sup>34</sup> The alternative solution does not require the search coil, and it is based solely on simultaneous input voltage and coil current measurements; however, the primary coil resistance value must be provided for the flux linkage accurate extraction of the flux data. The search coil approach is rid of the disadvantage and was selected by the authors in this series of the experiments. To acquire the information, each coil was subjected to sinusoidal voltage input excitations at the frequency  $f=1$  Hz. The magnitude of the voltage was adjusted to result in peak current levels within the range from 0 to 6 A. The induced voltages were measured simultaneously at each

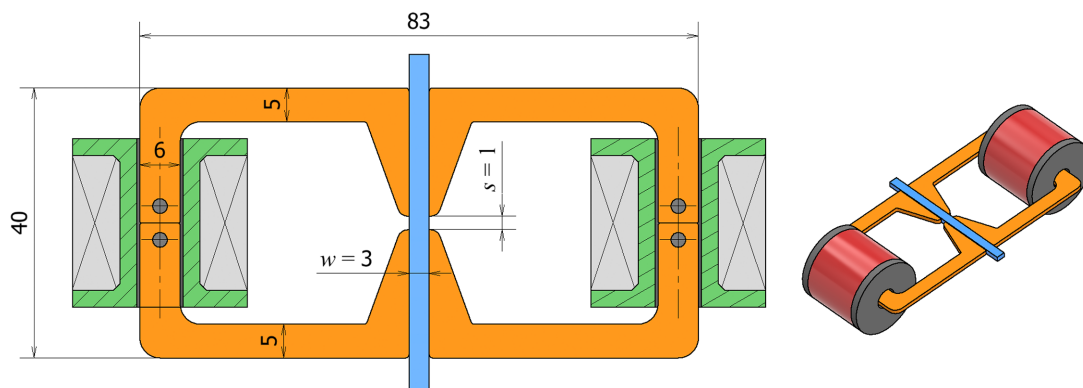


FIG. 12. Magnetic circuit geometry of the MR pinch valve and 3D view.

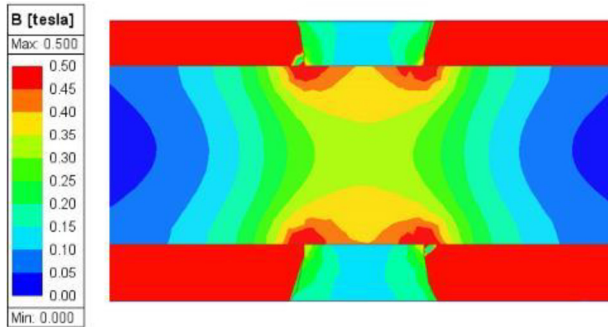


FIG. 13. Magnetic flux density distribution in the active zone.

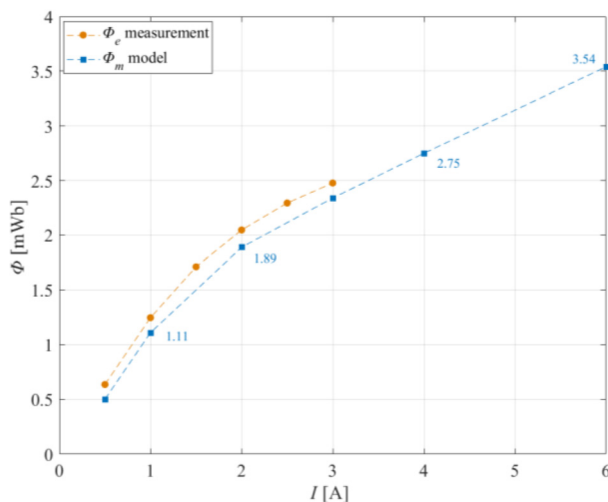


FIG. 14. FE model verification—measured (calculated) magnetic flux vs total current.

search coil and then integrated to yield magnetic flux time histories  $\phi(t)$ . The current signals were acquired with FLUKE I30S current probes, and in line with the input voltage data recorded on a PC via a Speedgoat real-time target machine fitted with 16-bit A/D I/O modules. The summary of the results can be found in Subsection 3 of the Appendix. The experiment was performed at no flow (static) conditions.

### 3. Results

Figure 13 reveals the magnetic flux density  $B$  distribution in the active zone at the highest magnetic flux level ( $\Phi = 3.54$  mWb) with MR fluid in the active zone. The presented magnetic data are scaled to the same dimensions (windows) as the imaging data (visualization). The magnetic flux density map shows that the flux density maximum values are at the wall. The smallest values are determined in the middle of the channel. The data were compared against the search coil measurements.

Figure 14 shows the magnetic flux  $\Phi_m$  (model) vs the measured flux  $\Phi_e$ . The agreement between the experiment and the magnetic model is very good within the specified current range. However, it is

expected that larger differences may arise in flow conditions. This would be probably caused by a change in MR fluid permeability due to particle movement induced by the magnetic flux density gradient.

### REFERENCES

- J. Rabinow, "The magnetic fluid clutch," *Trans. Am. Inst. Electr. Eng.* **67**, 1308 (1948).
- J. de Vicente, D. J. Klingenberg, and R. Hidalgo-Alvarez, "Magnetorheological fluids: A review," *Soft Matter* **7**, 3701 (2011).
- J. R. Morillas and J. de Vicente, "On the yield stress in magnetorheological fluids: A direct comparison between 3D simulations and experiments," *Composites, Part B* **160**, 626 (2019).
- O. Macháček, M. Kubík, Z. Strecker, J. Roupec, and I. Mazúrek, "Design of a frictionless magnetorheological damper with a high dynamic force range," *Adv. Mech. Eng.* **11**, 168781401982744 (2019).
- J. Yang, S. Sun, S. Ezani, N. Gong, L. Deng, S. Zhang, and W. Li, "New magnetorheological engine mount with controllable stiffness characteristics towards improved driving stability and ride comfort," *Smart Mater. Struct.* **31**, 125009 (2022).
- M. Kumar, A. Kumar, A. Alok, and M. Das, "Magnetorheological method applied to optics polishing: A review," *IOP Conf. Ser.: Mater. Sci. Eng.* **804**, 012012 (2020).
- M. R. Jolly, J. W. Bender, and J. D. Carlson, "Properties and applications of commercial magnetorheological fluids," *J. Intell. Mater. Syst. Struct.* **10**, 5 (1999).
- G. Z. Yao, F. F. Yap, G. Chen, W. H. Li, and S. H. Yeo, "MR damper and its application for semi-active control of vehicle suspension system," *Mechatronics* **12**, 963 (2002).
- N. D. Nguyen, T. Le-Duc, L. D. Hiep, and Q. H. Nguyen, "Development of a new magnetorheological fluid-based brake with multiple coils placed on the side housings," *J. Intell. Mater. Syst. Struct.* **30**, 734 (2019).
- S. Pisetskiy and M. Kermani, "High-performance magneto-rheological clutches for direct-drive actuation: Design and development," *J. Intell. Mater. Syst. Struct.* **32**, 2582 (2021).
- X. Gong, X. Ruan, S. Xuan, Q. Yan, and H. Deng, "Magnetorheological damper working in squeeze mode," *Adv. Mech. Eng.* **6**, 410158 (2014).
- F. D. Goncalves and J. D. Carlson, "An alternate operation mode for MR fluids—Magnetic gradient pinch," *J. Phys.: Conf. Ser.* **149**, 012050 (2009).
- J. D. Carlson, F. D. Goncalves, M. D. Catanzarite, and R. D. Dobbs, U.S. patent 2008/0060710 A1 (13 March 2007).
- H. E. Merritt, *Hydraulic Control Systems* (John Wiley and Sons Inc, 1967).
- J. Goldasz and B. Sapiński, "Magnetostatic analysis of a pinch mode magnetorheological valve," *Acta Mech. Autom.* **11**, 229 (2017).
- J. Goldasz, K. Kluszczynski, and B. Sapiński, in *19th International Conference on Research and Education in Mechatronics* (IEEE, 2018), pp. 48–51.
- M. Kubík, J. Goldasz, O. Macháček, Z. Strecker, and B. Sapiński, "Magnetorheological fluids subjected to non-uniform magnetic fields: Experimental characterization," *Smart Mater. Struct.* **32**, 035007 (2023).
- T.-H. Lee, G.-H. Kang, and S.-B. Choi, "A quasi-static model for the pinch mode analysis of a magnetorheological fluid flow with an experimental validation," *Mech. Syst. Signal Process.* **134**, 106308 (2019).
- M. Kubík, D. Pavlíček, O. Macháček, Z. Strecker, and J. Roupec, "A magnetorheological fluid shaft seal with low friction torque," *Smart Mater. Struct.* **28**, 047002 (2019).
- Y. Mizutani, H. Sawano, H. Yoshioka, and H. Shinno, "Magnetic fluid seal for linear motion system with gravity compensator," *Proc. CIRP* **33**, 581 (2015).
- P. Kuzhir, G. Bossis, V. Bashtovoi, and L. Vékás, "Capillary flow of a suspension of non-magnetic particles in a ferrofluid under highly non-uniform magnetic field," *Int. J. Multiphase Flow* **31**, 201 (2005).
- J. Goldasz, B. Sapiński, M. Kubík, O. Macháček, and W. Bankosz, in *10th ECCOMAS Thematic Conference on Smart Structures and Materials* (Department of Mechanical Engineering & Aeronautics University of Patras, Patras, 2023), pp. 1373–1380.
- L. Yongzhi, L. Xinhua, and L. Hao, "The Monte Carlo simulation to magnetic particles of magnetorheological fluids," *Proc. Eng.* **15**, 3896 (2011).

- <sup>24</sup>C. Fernandes and S. A. Faroughi, “Particle-level simulation of magnetorheological fluids: A fully-resolved solver,” *Int. J. Multiphase Flow* **169**, 104604 (2023).
- <sup>25</sup>N. Wang, X. Liu, S. Sun, G. Królczyk, Z. Li, and W. Li, “Microscopic characteristics of magnetorheological fluids subjected to magnetic fields,” *J. Magn. Mater.* **501**, 166443 (2020).
- <sup>26</sup>Y. Shen, D. Hua, X. Liu, W. Li, G. Krolczyk, and Z. Li, “Visualizing rheological mechanism of magnetorheological fluids,” *Smart Mater. Struct.* **31**, 025027 (2022).
- <sup>27</sup>D. Ji, Y. Luo, H. Ren, D. Wei, and J. Shao, “Numerical simulation and experimental analysis of microstructure of magnetorheological fluid,” *J. Nanomater.* **2019**, 6312606.
- <sup>28</sup>M. Ocalan and G. H. McKinley, “Rheology and microstructural evolution in pressure-driven flow of a magnetorheological fluid with strong particle–wall interactions,” *J. Intell. Mater. Syst. Struct.* **23**, 969 (2012).
- <sup>29</sup>Y. Yang and J. Huang, in *8th Annual IEEE International Conference on Nano/Micro Engineered and Molecular Systems (NEMS 2013)* (IEEE, 2013), Vol. 2, p. 1014.
- <sup>30</sup>M. Kubik, J. Goldasz, O. Machacek, and B. Sapinski, in *ACTUATOR 2022; International Conference and Exhibition on New Actuator Systems and Applications* (IEEE, 2022), pp. 1–3.
- <sup>31</sup>P. Kuzhir, M. T. López-López, and G. Bossis, “Abrupt contraction flow of magnetorheological fluids,” *Phys. Fluids* **21**(5), 053101 (2009).
- <sup>32</sup>J. Žáček, J. Goldasz, B. Sapinski, M. Sedláčik, Z. Strecker, and M. Kubík, “Assessment of the dynamic range of magnetorheological gradient pinch-mode prototype valves,” *Actuators* **12**, 449 (2023).
- <sup>33</sup>A. Munaz, M. J. A. Shiddiky, and N.-T. Nguyen, “Magnetophoretic separation of diamagnetic particles through parallel ferrofluid streams,” *Sens. Actuators, B* **275**, 459 (2018).
- <sup>34</sup>T. W. Nehl, S. Gopalakrishnan, and F. Deng, U.S. patent application 2007/0285195 A1 (13 December 2007).